https://doi.org/10.5194/egusphere-2026-5773
Preprint. Discussion started: 6 November 2026
© Author(s) 2026. CC BY 4.0 License.

Implementation of MEGAN v3.2 in SURFEX v9.0: A new framework for global biogenic emission simulations

Romain Salignat[1], Jonathan Américc[1], and Joaquim Arteta[1]
[1]Météo-France, CNRS, Univ. Toulouse, CNRM, Toulouse, France.
Correspondence: Joaquim Arteta (joaquim.arteta@meteo.fr)

Abstract. Biogenic volatile organic compounds (BVOCs), and isoprene in particular, strongly influence tropospheric chemistry, air quality, and climate feedbacks, making their accurate representation essential in atmospheric chemistry and climate modelling. However, simulated global isoprene budgets remain highly uncertain, spanning a wide range across models due to differences in emission factor datasets, land-surface descriptions, and environmental stress parametrizations. A recent study implemented the MEGAN v2.1 biogenic emission model within the SURFEX land-surface model, but this framework did not include developments introduced in MEGAN v3.2 or updates to SURFEX itself. Here we present the implementation and evaluation of MEGAN v3.2 within SURFEX v9.0 and compare it with the former MEGAN v2.1 - SURFEX v8.1 configuration. Global offline simulations for 2019 were performed using two meteorological forcing datasets to assess the sensitivity of simulated isoprene emissions to the MEGAN upgrade, soil moisture stress, emission factor parametrization, and land-cover description. Specifically, the transition from MEGAN v2.1 to v3.2 strongly reduces global annual isoprene emissions, yielding totals of 216-318 $\mathrm{Tg\,yr^{-1}}$, primarily driven by the updated gridded emission factor dataset prescribing lower emission potentials across most land regions. These lower totals are nonetheless consistent with recent evidence suggesting that MEGAN v2.1 overestimates emission potentials for certain vegetation types, and the spatial distribution and seasonal variability of isoprene remain largely preserved, indicating that the upgrade mainly rescales emission magnitudes rather than reorganizing global emission patterns. Sensitivity experiments further demonstrate that emission factor parametrization and land-cover description constitute first-order controls on simulated isoprene budgets, with associated uncertainties exceeding those related to meteorological forcing. The upgraded SURFEX-MEGAN framework therefore provides a robust basis for future coupled atmospheric chemistry applications.

1 Introduction

Volatile organic compounds (VOCs) are key gases of the Earth's atmosphere, with important effects on atmospheric oxidation capacity, air quality, and climate. Through their oxidation, VOCs contribute to the formation of secondary organic aerosols (Hallquist et al., 2009; Carlton et al., 2009; Carslaw et al., 2010) and ozone (Dreyfus et al., 2002; Guo et al., 2012; Wang et al., 2019), thereby influencing both the Earth's radiative balance and human health (IPCC, 2021). On a global scale, about 90 % of VOC emissions is estimated to originate from natural sources (Guenther et al., 1995, 2006), i.e., predominantly as biogenic volatile organic compounds (BVOCs). Among these, isoprene is the dominant compound, accounting for nearly half of total

https://doi.org/10.5194/egusphere-2026-5773
Preprint. Discussion started: 6 November 2026
© Author(s) 2026. CC BY 4.0 License.

BVOC emissions worldwide (Guenther et al., 2012). A robust representation of isoprene and other BVOC emissions from the diversity of terrestrial ecosystems is therefore required to accurately simulating their impacts on atmospheric composition, and climate feedbacks.

Despite their importance, ground-based measurements provide valuable process-level constraints from the leaf to the canopy scale (Sarkar et al., 2020; Rocco et al., 2024), but their limited spatiotemporal coverage prevents them to fully constraining BVOC fluxes at larger scales (Arneth et al., 2011). For instance, these emissions are heavily controlled by vegetation characteristics (Lathière et al., 2006; Sindelarova et al., 2022) and environmental conditions (Rinne et al., 2002; Jiang et al., 2018), whose drivers vary strongly across ecosystems and over time, resulting in significant regional and global differences in BVOC emissions. Furthermore, in the context of climate change (increasing temperatures, rising CO_2 concentrations, and land-use changes), these drivers are expected to seriously influence BVOC emissions (Heald et al., 2009; Peñuelas and Staudt, 2010; Pacifico et al., 2012; Stavrakou et al., 2014), but the magnitude and even the direction of these changes stand highly uncertain. This combination of biological and environmental complexity therefore remains a major source of uncertainty in estimating present-day emissions and their long-term trends.

To account for this variability, and to assess BVOC emissions at regional to global scales, process-based emission models have been developed. BVOC emission estimates rely either on top-down approaches (Palmer et al., 2006; Harrison et al., 2012) which use atmospheric observations to infer surface fluxes, or on bottom-up approaches (Guenther et al., 1995; Lathière et al., 2006) that combine land-cover information, emission factors, and environmental activity algorithms. Among bottom-up approaches, the Model of Emissions of Gases and Aerosols from Nature (MEGAN) has become one of the most widely used frameworks (Guenther et al., 1995, 2006, 2012) for simulating BVOC emissions at regional and global scales (Müller et al., 2008; Stavrakou et al., 2014; Sindelarova et al., 2014, 2022; Messina et al., 2016; Oumami et al., 2024). Precisely, MEGAN combines emission factors, which describe the intrinsic emission potential of vegetation, with activity factors that account for environmental controls such as light, temperature, leaf age, soil moisture, and atmospheric composition (Guenther et al., 2012). Reported global isoprene totals from MEGAN-based studies range from about 350 to 800 $\mathrm{Tg\,yr^{-1}}$ (Guenther et al., 2012; Messina et al., 2016; Henrot et al., 2017; Sindelarova et al., 2022), illustrating a strong sensitivity of modelled BVOC fluxes to input data and model formulation. Thus, these differences highlight the need for improved emission models and updated parametrizations to better represent vegetation processes and environmental responses in BVOC emission modelling.

Despite its widespread use, MEGAN still presents several limitations related to the representation of vegetation processes, environmental stress responses, and canopy-scale processes. In particular, uncertainties remain in emission factors, while canopy heterogeneity and several stress-related processes or compounds are either missing or represented using simplified parametrizations (Guenther et al., 2019). As a result, different implementations of MEGAN often rely on different vegetation datasets, canopy parametrizations, meteorological forcings, and chemical speciation mappings, which contributes to a large spread in simulated emissions. For instance, some model evaluation studies have also reported widespread positive biases in modelled isoprene emissions, partly attributed to uncertainties in emission factors and vegetation representations (Jiang et al., 2019; Ciarelli et al., 2024; Bettineschi et al., 2026). More generally, the representation of vegetation stress processes remains incomplete in current BVOC emission models. Processes such as leaf senescence (Vermeuel et al., 2023), drought stress (Seco

https://doi.org/10.5194/egusphere-2026-5773
Preprint. Discussion started: 6 November 2026
© Author(s) 2026. CC BY 4.0 License.

et al., 2015; Opacka et al., 2022; Wang et al., 2022), or extreme weather events (Riches et al., 2022) can significantly affect BVOC emissions, but they are still poorly constrained by observations and remain difficult to represent in models. These limitations contribute to the overall uncertainty in current BVOC emission estimates and motivate the development of improved model formulations.

To address some of these limitations, a new version of MEGAN (v3.2) has recently been developed, introducing an updated representation of vegetation processes, improved environmental response algorithms, and a revised emission factor database (Guenther et al., 2019). This version also relies on an updated pre-processing framework that derives gridded emission potentials from high-resolution information on vegetation distribution and species composition. First applications of MEGAN v3.2 at regional and global scales indicate that the updated framework can modify both the magnitude and spatial distribution of emissions compared with earlier versions, with important implications for atmospheric chemistry simulations (Wang et al., 2024; Li et al.; Bettineschi et al., 2026). For example, Wang et al. (2024) used MEGAN v3.2 to estimate global BVOC emissions over the 2001-2020 period and reported isoprene emissions on the lower end of the previously published range. In addition, Cholakian et al. (2023) showed that revised emission factors combined with more realistic vegetation information can improve agreement between modelled and observed BVOC concentrations. These developments make MEGAN v3.2 a promising framework for updated online coupling in land-surface and atmospheric chemistry models.

Within this context, Oumami et al. (2024), first implemented MEGAN v2.1 in the SURFace EXternalisée (SURFEX) land surface modelling platform and evaluated the coupled system at the global scale. That study demonstrated the feasibility and relevance of coupling a biogenic emission model directly to SURFEX in order to compute emissions consistently with surface prognostics and land-atmosphere interactions. However, this implementation relied on an older version of MEGAN and did not benefit from the developments introduced in MEGANv3.2 or from updates in the SURFEX modelling framework. Updating this coupling therefore represents a logical next step toward implementing the representation of BVOC emissions in the SURFEX environment.

The objective of the present study is to implement MEGAN v3.2 in SURFEX v9.0, building on the coupling strategy of Oumami et al. (2024), and to document the methodological developments associated with this update. A particular attention is given to the integration of the new MEGAN pre-processing framework and environmental response functions, the consistency between SURFEX vegetation variables and MEGAN input requirements, and the preservation of backward compatibility with the previous SURFEX-MEGAN framework. This paper describes the new implementation, evaluates the impact of upgrading from MEGAN v2.1 to v3.2 on BVOC emissions, and discusses the implications for global isoprene emission estimates. Section 2 describes the SURFEX v9.0 and MEGAN v3.2 model coupling strategy, along with the experimental setup and input data. Section 3 illustrates the experimental setup, evaluates the new framework, and discusses the implications and limitations of the new implementation.

https://doi.org/10.5194/egusphere-2026-5773
Preprint. Discussion started: 6 November 2026
© Author(s) 2026. CC BY 4.0 License.

2 Model description and implementation

This study builds on the coupling framework introduced by Oumami et al. (2024) and updates it by implementing MEGAN v3.2 into the SURFEX v9.0 land surface modelling platform. The SURFEX-MEGAN system allows biogenic emissions to be calculated from detailed vegetation-dependent inputs, ensuring consistency between land-atmosphere exchanges and emission processes. This section outlines the SURFEX model (Sect. 2.1), the MEGAN emission model (Sect. 2.2), and the coupling strategy between the two models (Sect. 2.3).

2.1 SURFEX version 9.0 land surface model

SURFEX (SURFace EXternalisée) v9.0, developed by Météo-France, is a land surface modeling platform designed to simulate surface-atmosphere interactions and includes the representation of surface processes relevant to chemistry and aerosols. Note that a comprehensive scientific description of SURFEX is already provided in Le Moigne (2018), while its coupling with MEGAN is described in Oumami et al. (2024). Only a brief overview is given here.

In SURFEX, each atmospheric model grid cell is represented as a combination of four surface tiles: nature, town, sea/ocean, and lakes. Surface-atmosphere exchanges are computed separately for each tile using dedicated physical schemes, and the total flux exchanged with the atmosphere is thereafter calculated as the area-weighted average of the tile contributions. In particular, over natural surfaces, SURFEX uses ISBA (Interaction between Soil, Biosphere, and Atmosphere) land surface model (Noilhan and Planton, 1989; Calvet et al., 1998), that simulates exchanges of energy and water between the soil, vegetation, and the atmosphere. The ISBA variables are necessary to drive the MEGAN emission model, ensuring consistency between land surface conditions and BVOC emissions. However, note that when SURFEX is run in offline mode, a forcing file is required to provide the essential meteorological and radiation data (temperature, specific humidity, CO_2, solar radiation, etc.).

The vegetation and land-cover properties in SURFEX are prescribed from the ECOCLIMAP database (Faroux et al., 2013). In SURFEX v9.0, the model also supports the new ECOCLIMAP-SG (Druel et al., 2022), which provides an improved global description of plant functional types (PFTs) and leaf area index (LAI) at 300 m spatial resolution. Compared with earlier versions, this update is expected to better represent sub grid-scale land surface heterogeneity, which is particularly important for biogenic emission estimates because they strongly depend on vegetation distribution, density, and seasonality. Furthermore, beyond database updates, SURFEX v9.0 also includes technical and physical improvements relative to earlier versions, which may affect the meteorological and surface variables used to drive biogenic emissions. All these new developments make version 9.0 a relevant framework for revisiting the MEGAN coupling originally proposed by Oumami et al. (2024).

2.2 MEGAN version 3.2 biogenic emission model

2.2.1 MEGAN overview

MEGAN (Model of Emissions of Gases and Aerosols from Nature) v3.2, described by Guenther et al. (2019), is implemented here within SURFEX to estimate net emissions of 201 speciated biogenic volatile organic compounds and other trace species

https://doi.org/10.5194/egusphere-2026-5773
Preprint. Discussion started: 6 November 2026
© Author(s) 2026. CC BY 4.0 License.

from terrestrial vegetation to the atmosphere. MEGAN is a process-based modelling system established by Guenther et al. (1991, 1993, 1995) that estimates biogenic emissions as a function of vegetation type and environmental conditions, also embedding a multi-layer canopy module that explicitly represents vegetation layers, and computes prognostics variables such as vegetation temperature, and radiation within canopy.

In MEGAN, the emission flux F of a given biogenic compound j can be simply expressed as:

$$F_j = \gamma_i \times EF_j \tag{1}$$

where F_j is the biogenic emission flux ($\mathrm{nmol\,m^{-2}\,s^{-1}}$) of speciated species j, EF_j is the emission factor under standard conditions ($\mathrm{nmol\,m^{-2}\,s^{-1}}$) calculated for each j speciated species, and γ_i is a dimensionless activity factor, computed for i lumped species (i=19 in MEGAN v3.2), accounting for deviations (see Eq. 2) from standard conditions due to environmental and physiological drivers.

The 19 MEGAN v3.2 lumped species are isoprene ($ISOP$), 2-methyl-3-buten-2-ol (MBO), α-pinene-like monoterpenes (MT_PINE), acyclic monoterpenes (MT_ACYC), camphene-like monoterpenes (MT_CAMP), sabinene-like monoterpenes (MT_SABI), aromatic monoterpenes (MT_AROM), nitric oxide (NO), highly reactive sesquiterpenes (SQT_HR), less reactive sesquiterpenes (SQT_LR), methanol ($MEOH$), acetone ($ACTO$), ethanol ($ETOH$), organic acids ($ACID$), low-volatility organic compounds ($LVOC$), oxidized products ($OXPROD$), stress-induced compounds ($STRESS$), carbon monoxide (CO), and other volatile organic compounds ($OTHER$).

2.2.2 Emission activity factor

In MEGAN v3.2, the emission activity factor γ_i is formulated as the product of several response functions. These include newly introduced or revised processes, such as strong wind events (γ_{HW} for wind speeds exceeding $12\,\mathrm{m\,s^{-1}}$), extreme temperatures responses (γ_{LT} and γ_{HT}, for temperatures lower than 10 °C or higher than 40 °C, respectively), air-quality stress associated with ozone exposure (γ_{AQ} for ozone exposure larger than $20\,\mathrm{ppm\,h}$), an updated canopy radiation and temperature response (γ_{TP}), and a bi-directional exchange LAI response (γ_{BD}) for specific compounds (e.g., ethanol and acetaldehyde, i.e., the $ETOH$ lumped species). In addition, previously established response functions (from MEGAN v2.1) are preserved, including the effects of leaf age (γ_{AGE}) and soil moisture stress (γ_{SMT}), or atmospheric CO_2 (γ_{CO2} for concentrations superior to 400 ppm) for isoprene emissions. In simplified form, the emission activity factor for each lumped species i is calculated as:

$$\gamma_i = LAI \times \gamma_{TP} \times \gamma_{AGE} \times \gamma_{HW} \times \gamma_{LT} \times \gamma_{HT} \times \gamma_{AQ} \times \gamma_{SMT} \times \gamma_{CO2} \times \gamma_{BD} \tag{2}$$

where LAI is the current leaf area index (dimensionless) that reflects the vegetation seasonality.

2.2.3 Emission potential factor

In Eq. (1), the emission factor EF_j represents the intrinsic emission potential of a given vegetation type for a specific compound j under prescribed reference conditions:

$$EF_j = \varepsilon_i^{map} \times \chi_j \tag{3}$$

https://doi.org/10.5194/egusphere-2026-5773
Preprint. Discussion started: 6 November 2026
© Author(s) 2026. CC BY 4.0 License.

where ε_i^{map} represents gridded emission potential maps ($\mathrm{nmol\,m^{-2}\,s^{-1}}$) for each lumped species, and χ_j the species j speciation. Note that in MEGAN v3.2, species speciation χ_j is no longer dependent on PFT compositions, and that EF_j are now prescribed only via ε_i^{map} (i.e., PFT-dependent emission potentials are no longer existing, see Sect. 2.3) generated using the new MEGAN emission factor pre-processor (downloaded at https://drive.google.com/file/d/1ZAkE1osXK6Gl0GEzfGyTDGm17PfwfxDL/view, last access: 18 March 2026). More precisely, the pre-processor produces gridded emission factor maps (ε_i^{map}) from high-resolution input datasets describing growth form, ecotype, speciation, and emissions factors for individual plant types, which are then aggregated to the target model grid resolution. The high-resolution input datasets used in this work were obtained from the MEGAN v3.2 database repository (https://zenodo.org/records/10939297, last access: 18 March 2026). An explicit description of the new MEGAN emission factors pre-processor is available in Hamer et al. (2026).

2.2.4 Other model updates

Compared with MEGAN v2.1, version 3.2 introduces several other important updates. The model now estimates emissions for 19 chemical compound classes (instead of 20 in v2.1), which are subsequently redistributed into 201 distinct biogenic species (compared to 150 in v2.1) or output in chemical categories associated with various atmospheric chemistry mechanisms. The representation of vegetation has also been revised, with emissions now calculated based on a reduced set of 6 canopy types, instead of the 16 PFTs used in MEGAN v2.1, leading to repercussions on γ_i and EF_j calculations. Lastly, as MEGAN v3.2 includes updates to environmental activity algorithms and introduces new parametrizations for several stress-related processes (Sect. 2.2.2), along with a revised emission factor database, and the implementation of an updated pre-processing framework to derive gridded emission potentials from high-resolution vegetation information (Sect. 2.2.3), these developments motivate the implementation of MEGAN v3.2 within SURFEX, with the objective of improving the representation of BVOC emissions and their response to environmental drivers in land-atmosphere modelling systems.

2.3 Implementation of MEGAN v3.2 in SURFEX v9.0

The implementation performed in this study follows the general online coupling strategy proposed by Oumami et al. (2024), in which MEGAN is embedded within SURFEX so that biogenic emissions are calculated interactively from surface and vegetation states simulated by the land surface model. In the present work, both the host model (SURFEX) and the emission model (MEGAN) are updated, requiring adaptation of the interface to SURFEX v9.0 together with the implementation of the MEGAN v3.2 formulations and revised input datasets.

This updated implementation benefits from the improved representation of vegetation provided by ECOCLIMAP-SG, especially for PFT distributions and LAI (Munier et al., 2018), which are key inputs for the SURFEX-MEGAN coupling. Because biogenic emissions are highly sensitive to vegetation structure and environmental forcings, the combined use of SURFEX v9.0 and MEGAN v3.2 is expected to provide a more consistent and up-to-date framework for global biogenic emission estimates.

Yet, as MEGAN v3.2 now relied on a reduced set of 6 canopy types (Sect. 2.2.4), a specific correspondence between the 19 SURFEX land type description and the new 6 MEGAN canopy types need to be established (Table 1). Precisely, among the natural vegetation types (NVTs) proposed in SURFEX, three types correspond to non-vegetated surfaces (bare soil, rock, and

https://doi.org/10.5194/egusphere-2026-5773
Preprint. Discussion started: 6 November 2026
© Author(s) 2026. CC BY 4.0 License.

permanent snow) and are therefore assigned no MEGAN canopy type. The remaining 16 vegetated NVTs are mapped onto the 6 canopy types used in MEGAN v3.2 ensuring consistency between the vegetation description used in SURFEX and that required by MEGAN for emission calculations.

Table 1. Correspondence between the 19 natural vegetation types (NVTs) of SURFEX and the 6 canopy types used in MEGAN v3.2. The index k denotes the NVT number used internally in SURFEX and referenced in subsquent Eq. 4 and Table S1. Non-vegetated NVTs ($k = 1, 2, 3$) carry no MEGAN canopy type assignment.

k	SURFEX NVT code	SURFEX NVT name	MEGAN v3.2 canopy types
1	NVT_{NO}	no vegetation (smooth)	
2	NVT_{ROCK}	no vegetation (rocks)	-
3	NVT_{SNOW}	permanent snow and ice	
5	NVT_{BONE}	Needleleaf evergreen boreal trees	
15	NVT_{TENE}	Needleleaf evergreen temperate trees	Needleleaf trees
17	NVT_{BOND}	Needleleaf deciduous boreal trees	
6	NVT_{TRBE}	Broadleaf evergreen tropical trees	Tropical forest trees
13	NVT_{TRBD}	Broadleaf deciduous tropical trees	
4	NVT_{TEBD}	Broadleaf deciduous temperate trees	
14	NVT_{TEBE}	Broadleaf evergreen temperate trees	Temperate broadleaf trees
16	NVT_{BOBD}	Broadleaf deciduous boreal trees	
19	NVT_{SHRB}	Shrub	Shrubs
10	NVT_{GRAS}	Grassland	
11	NVT_{TROG}	Tropical grass	Herbaceous
12	NVT_{PARK}	Irrigated grass*	
18	NVT_{BOGR}	Boreal grass	
7	NVT_{C3}	Winter crops	
8	NVT_{C4}	Summer crops	Crops
9	NVT_{IRR}	Irrigated crops*	

*described NVTs introduced by ECOCLIMAP-SG

190 In addition, while the standard MEGAN v3.2 framework relied only on gridded emission factor maps (ε_i^{map}) derived from the MEGAN pre-processor (Sect. 2.2.3), the earlier MEGAN v2.1 also allowed emissions to be calculated from PFT-dependent emissions factors (ε_k). This option was important to account for evolving vegetation properties, particularly changes in PFT fractions and LAI. To preserve this central capability, a PFT-dependent emission factor option was reintroduced (Eq. 4) in the

https://doi.org/10.5194/egusphere-2026-5773
Preprint. Discussion started: 6 November 2026
© Author(s) 2026. CC BY 4.0 License.

present implementation:

$$EF_j = \chi_j \times \frac{\sum_{k=4}^{19}(\varepsilon_{k,i} \times f_k)}{\sum_{k=4}^{19}(f_k)} \quad (4)$$

where f_k symbolizes the PFT composition of the grid cell, and $\varepsilon_{k,i}$ the PFT-dependent emission factors for each i lumped species. This required the creation of a new table of PFT-dependent emission factors (Table S1), consistent with the new 19 lumped compounds classes represented in MEGAN v3.2. These values were derived from the high-resolution input datasets used with the MEGAN emission factor pre-processor (Sect. 2.2.3) and assigned to each 16 canopy types for all modelled lumped species (values would be thereafter redistributed consistently to the 6 new PFTs). However, note that the two new ECOCLIMAP-SG NVTs do not have yet specific emission factor values, and are therefore not considered in this method. Instead, NVT_{SHRUB} are on the contrary subdivided into 3 NVTs corresponding to distinct geographical areas (polar, temperate, and tropical, see Table S1). Broadly, this new dataset produces spatial pattern of isoprene emission potentials similar to those of the previous version (Pearson r = 0.85), but globally reduced values (-66 %), consistent with the downward revision also observed in the updated ε^{map}_{ISOP} dataset.

Likewise, the additional response functions to environmental and physiological drivers introduced in MEGAN v3.2, including those related to strong wind events, extreme temperatures, air-quality stress, and bi-directional exchange LAI response (γ_{HW},γ_{HT},γ_{LT},γ_{AQ},γ_{BD}), were implemented in the coupled system alongside the pre-existing activity factors (Sect. 2.2). The formulation of the canopy radiation and temperature response (γ_{TP}) was also revised accordingly. Finally, the updated speciation mapping introduced in MEGAN v3.2 was implemented to convert emissions from MEGAN compound classes to the species used in atmospheric chemistry mechanisms.

3 Evaluation of the coupled SURFEX-MEGAN model

3.1 Baseline simulation

To isolate the impact of the MEGAN version upgrade from that of the SURFEX version change, MEGAN v2.1 was first migrated into SURFEX v9.0. This intermediate configuration serves as a bridge simulation (called Baseline simulation, see Tables 2 and 3) and allows to verify that the transition from SURFEX v8.1 to v9.0 does not introduce unintended biases in the natural-tile physics relevant to biogenic emissions.

The Baseline simulation was based on the coupled version described by Oumami et al. (2024), while keeping the MEGAN v2.1 settings as close as possible to the original configuration (Table 2). In particular, γ_{CO2} and γ_{SMT} were set to 1 (i.e. deactivated), emission factor maps from MEGAN v2.1 were used, and SURFEX v9.0 was run in offline considering only the nature tile (i.e., ISBA). ERA5 reanalysis meteorological forcing was used, and the simulation was performed globally for the year 2019, with 1 month spin-up (December 2018), at a horizontal spatial resolution of $1° \times 1°$. Although SURFEX v9.0 supports the high-resolution ECOCLIMAP-SG dataset (Sect. 2.1), ECOCLIMAP-I was retained here to ensure consistency with the reference configuration in Oumami et al. (2024).

https://doi.org/10.5194/egusphere-2026-5773
Preprint. Discussion started: 6 November 2026
© Author(s) 2026. CC BY 4.0 License.

Table 2. Baseline simulation (SURFEXv9.0-MEGANv2.1) configuration.

SURFEX-MEGAN processes	SURFEX option	References
Meteorological forcing	ERA5	Hersbach et al. (2023a, b)
Plant functional types (PFT)	ECOCLIMAP-I	Faroux et al. (2013)
Leaf area index (LAI)	ECOCLIMAP-I	Faroux et al. (2013)
Activity factors (γ_i)	γ_{CO2} and γ_{SMT} turned off	Guenther et al. (2012)
Emission potentials (EF_j)	MEGAN v2.1 ε_i^{map}	Oumami et al. (2024)

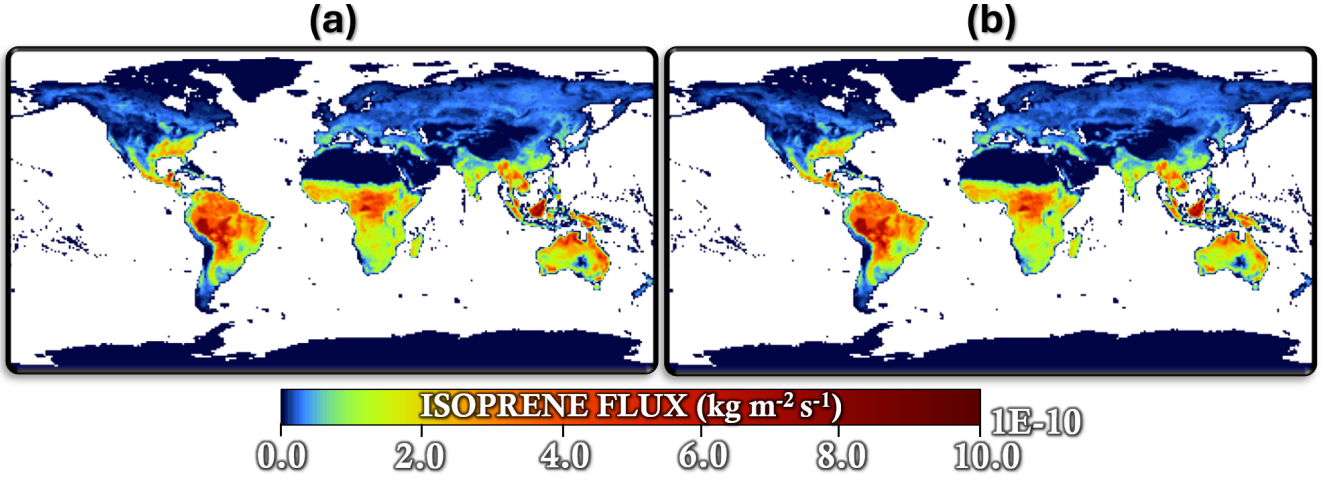


Figure 1. Spatial distribution of annual mean isoprene emission in $\mathrm{kg\,m^{-2}\,s^{-1}}$ simulated over 2019 using (a) SURFEX v8.1 (Oumami et al., 2024) and (b) SURFEX v9.0 (Baseline simulation) frameworks conducted with the ERA5 meteorological forcing.

Figure 1 compares the global annual isoprene emission fluxes obtained for 2019 with (a) SURFEX v8.1 - MEGAN v2.1 (Oumami et al., 2024) and (b) SURFEX v9.0 – MEGAN v2.1 (Baseline simulation). As shown in Fig. 1, the transition from SURFEX v8.1 to v9.0 induces only a small reduction in global annual isoprene emissions (-4.1 %), from 443.2 $\mathrm{Tg\,yr^{-1}}$ to 424.9 $\mathrm{Tg\,yr^{-1}}$, while leaving the spatial distribution of emission hotspots entirely unchanged (Pearson r = 1.00). The difference maps confirm that changes are of negligible magnitude (Fig. S1.a) and are confined to a limited number of regions (Fig. S1.b), with no detectable differences simulated over Europe, Africa, and South America. Still, the largest regional reductions are concentrated over Australia (-17.9 %), Russia (-7.8 %), North America (-7.0 %), and Southeast Asia (-6.5 %). Although the relative reduction over Australia appears large, the associated absolute differences remain well below $1.5 \times 10^{-10}\,\mathrm{kg\,m^{-2}\,s^{-1}}$, which is negligible compared to the simulated isoprene flux range (Fig. 1), thus confirming that the SURFEX upgrade contributes only slightly to the regional signals discussed in the subsequent sections. Yet, the precise mechanisms driving these regional differences remain difficult to identify, as several updates introduced in SURFEX v9.0 may have alter the near-surface

https://doi.org/10.5194/egusphere-2026-5773
Preprint. Discussion started: 6 November 2026
© Author(s) 2026. CC BY 4.0 License.

meteorological and radiative conditions controlling isoprene emissions. A detailed attribution of these regional changes to specific SURFEX v9.0 developments is, however, beyond the scope of the present study.

Overall, these results confirm that the SURFEX upgrade does not introduce significant biases in simulated isoprene emissions at the global scale, and that any spatial reorganisation and magnitude changes identified in subsequent experiments (see Sect. 3.2) can be attributed to the MEGAN upgrade rather than to changes in the land surface model itself.

3.2 SURFEX v9.0 - MEGAN v3.2 framework evaluation

The coupled SURFEX v9.0 – MEGAN v3.2 framework was used to perform global simulations of BVOC emissions for the year 2019, using a one-month spin-up period as described in Section 3.1. Unless otherwise stated, all the new developments presented in Section 2 were activated in the simulations (see Table 3). The air quality stress response (γ_{AQ}) and CO_2 inhibition response (γ_{CO2}) were nevertheless disabled because recent and spatially consistent forcing datasets were not available for these offline experiments.

Table 3. Overview of the different SURFEX-MEGAN simulations performed in the present work. Estimates of global annual isoprene fluxes (F_{ISO}) are displayed for the two meteorological forcings used in this study (i.e. ERA5/IFS).

Simulations	Land-cover database	Framework	Emission factors	Soil moisture activity factor	F_{ISO} ($\mathrm{Tg\,yr^{-1}}$)
Baseline	ECOCLIMAP-I	MEGANv2.1	ε_i^{map}	$\gamma_{SMT} = 1$	425/369
R1	ECOCLIMAP-I	MEGANv3.2	ε_i^{map}	$\gamma_{SMT} = 1$	318/289
R2	ECOCLIMAP-I	MEGANv3.2	ε_i^{map}	$\gamma_{SMT} \neq 1$	237/216
R3	ECOCLIMAP-I	MEGANv3.2	$\varepsilon_{k,i}$	$\gamma_{SMT} = 1$	240/233
R4	ECOCLIMAP-SG	MEGANv3.2	$\varepsilon_{k,i}$	$\gamma_{SMT} = 1$	262/290

To assess the sensitivity of the model to land-surface (Sect. 3.2.3) and meteorological (Sect. 3.2.4) inputs, simulations were conducted respectively using two land-cover databases (ECOCLIMAP-I and ECOCLIMAP-SG) and two meteorological forcing datasets (ERA5 and IFS). Emissions are estimated for the 23 species of the Regional Atmospheric Chemistry Mechanism (RACM; Stockwell et al., 1997), including isoprene (ISO), methane (CH4), and several lumped hydrocarbon and oxygenated compounds. Yet, only isoprene is discussed in this study. The mapping between MEGAN species and RACM species follows the methodology described by Guenther et al. (2019).

3.2.1 Evaluation of MEGAN v3.2 against MEGAN v2.1 in SURFEX v9.0

Figure 2 presents the global distribution of annual mean isoprene emissions simulated with the Baseline (Fig. 2.a) and R1 (Fig. 2.b) experiments, granting a direct visual comparison between MEGAN v2.1 and MEGAN v3.2 within SURFEX v9.0. This figure points out, in particular, that the transition to MEGAN v3.2 produces a large and spatially coherent reduction in isoprene emissions, with a global decrease of 25 % relative to the Baseline, yielding an annual total of 317.6 $\mathrm{Tg\,yr^{-1}}$ (see Table 3).

https://doi.org/10.5194/egusphere-2026-5773
Preprint. Discussion started: 6 November 2026
© Author(s) 2026. CC BY 4.0 License.

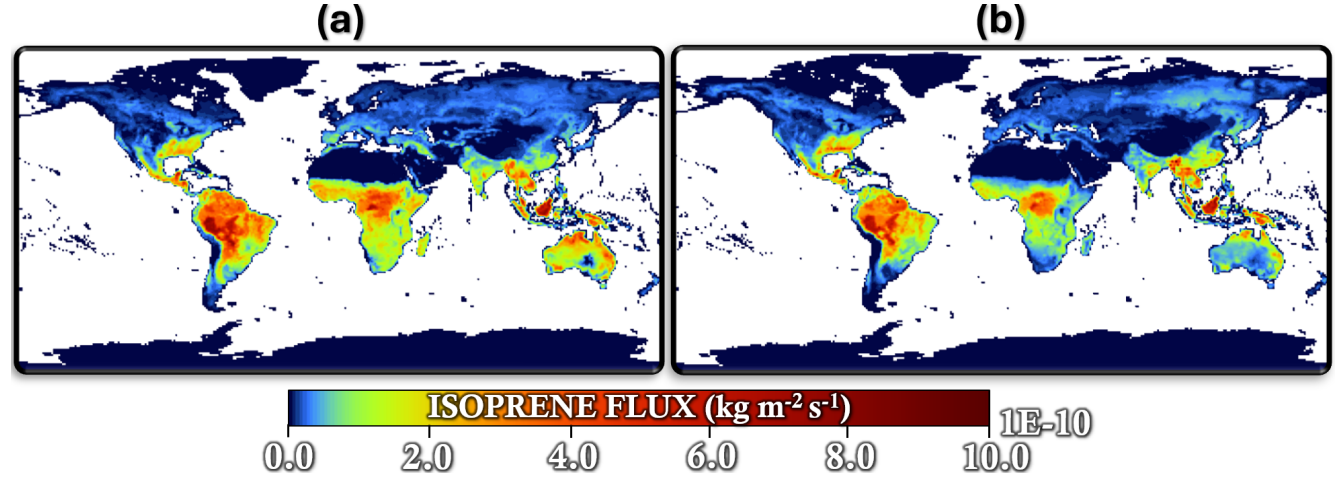


Figure 2. Spatial distribution of annual mean isoprene emission fluxes ($\mathrm{kg\,m^{-2}\,s^{-1}}$) simulated for 2019 using ERA5 reanalyses and conducted with the (a) Baseline and (b) R1 simulations.

Table 4. Regional isoprene emission totals and spatial statistics comparing the Baseline and R1 annual simulations for 2019 using the ERA5 meteorological forcing.

Region	Baseline ($\mathrm{Tg\,yr^{-1}}$)	R1 ($\mathrm{Tg\,yr^{-1}}$)	NMB (%)	Pearson r
Global	424.90	317.60	-25.20	0.94
Northern Hemisphere	204.10	165.70	-18.80	0.93
Southern Hemisphere	220.80	151.90	-31.20	0.95
North America	33.10	32.00	-3.30	0.96
South America	143.30	117.20	-18.20	0.96
Europe	8.70	6.20	-28.80	0.81
North Africa	6.00	2.30	-62.50	0.87
East Africa	95.00	59.80	-37.10	0.88
South Africa	17.80	8.50	-52.30	0.81
Russia	13.40	12.30	-8.10	0.78
Southeast Asia	64.60	62.20	-3.70	0.94
Australia	43.40	17.30	-60.10	0.86

Figure S2 further illustrates the absolute and relative differences between R1 and the Baseline simulation, while Table 4 summarizes emission totals and spatial statistics from the nine geographical regions defined in the GlobEmission project (https://www.globemission.eu/, last access: 02 July 2026). More specifically, the comparison reveals a marked hemispheric contrast (Fig. S2.a, and Table 4). Although the Southern Hemisphere represents only approximately 22 % of vegetation land grid cells, it contributes nearly 64.2 % of the global emission decrease (Table 4). In absolute terms, the Southern Hemisphere

https://doi.org/10.5194/egusphere-2026-5773
Preprint. Discussion started: 6 November 2026
© Author(s) 2026. CC BY 4.0 License.

decrease amounts to 68.9 $\mathrm{Tg\,yr^{-1}}$ compared to 38.4 $\mathrm{Tg\,yr^{-1}}$ in the Northern Hemisphere. Specifically, Australia (Fig. S2.b, and Table 4) exhibits both one of the strongest regional reductions (-60.1 %) and largest spatial reorganizations (Pearson r = 0.86), while Southeast Asia and North America show relatively small changes (-3.7 % and -3.3 % respectively).

Despite these regional differences, the globally high spatial Pearson correlation coefficient (Pearson r = 0.94) between the Baseline and R1 simulations (Table 4) indicates that the version upgrade primarily rescales isoprene emission magnitudes rather than reorganizing the geographical distribution of emission hotspots. This reduction seems to be mainly driven by the new gridded isoprene emission potential dataset (ε^{map}_{ISOP}) implemented in MEGAN v3.2. As shown in Fig. S3, the new dataset assigns essentially lower emission potentials across most tropical and Southern Hemisphere ecosystems, with absolute decreases reaching up to 35 $\mathrm{nmol\,m^{-2}\,s^{-1}}$ over Amazonia and central Africa. In contrast, localized increases are simulated over parts of central Asia and the eastern United States, consistent with the comparatively small emission reductions reported for these regions in Table 4.

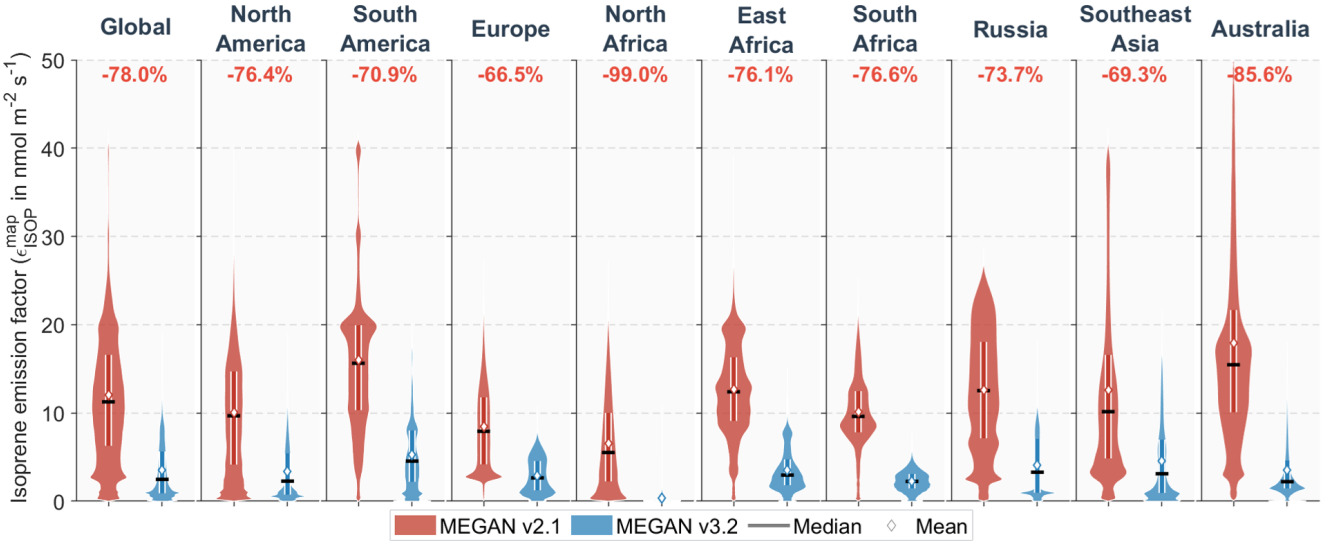


Figure 3. Violin plots showing the regional distributions of isoprene emission potentials (in $\mathrm{nmol\,m^{-2}\,s^{-1}}$) in MEGAN v2.1 and v3.2. Median ε^{map}_{ISOP} values for each region are painted using black solid lines, while mean values are drawn with white diamonds.

To further illustrate the decline in isoprene emission potentials, Fig. 3 describes the regional distributions of isoprene emission potentials in MEGAN v2.1 and v3.2 using violin plots. Across all regions, the updated dataset systematically shifts the distributions toward lower values, with a global median emission potential decrease of approximately 78 % (from 11.3 to 2.5 $\mathrm{nmol\,m^{-2}\,s^{-1}}$). The strongest reductions are observed over Australia (-85.6 %) and across african regions (-76.1 % to -99.0 %), in agreement with the large emission decreases simulated in experiment R1 over these territories. By contrast, temperate North America and Europe exhibit smaller distributional shifts, consistent with the more moderate emission reductions reported in Table 4. Hence, this spatial correspondence between the distributional shifts in emission potentials (Fig. 3) and

https://doi.org/10.5194/egusphere-2026-5773
Preprint. Discussion started: 6 November 2026
© Author(s) 2026. CC BY 4.0 License.

the regional emission response (Table 4) strongly suggests that the updated ε_{ISOP}^{map} is the primary driver of the global isoprene reduction in MEGAN v3.2.

Furthermore, the largest discrepancies between emission potentials reductions and emission responses are concentrated in arid and semi-arid regions. In particular, North Africa exhibits the strongest median emission potentials reduction of all regions (-99.0 %), yet isoprene emissions decrease by only 62.5 % (Table 4), illustrating the highly non-linear relationship between emission potential and simulated flux in this region. Similarly, Australia and South Africa show large potential reductions (-85.6 % and -76.6 % respectively) that translate into significant but proportionally smaller emissions decreases (-60.1 % and -52.3 %), consistent with the limited buffering capacity of activity factors in water-limited ecosystems where LAI and vegetation density are low. By contrast, North America exhibits the most pronounced non-linearity, with an emission potential reduction of -76.4 % producing only a -3.3 % change in isoprene emissions, suggesting here a strong compensating influence of temperature and radiation activity factors in this region that largely offsets the reduced emission potential. Overall, although emission potentials decrease considerably (-78.0 %), the corresponding reduction in simulated global isoprene emissions remains comparatively smaller (-25.2 %), reflecting primarily the buffering effect of environmental activity factors (temperature, LAI, and radiation) which sustain high emission rates over productive tropical ecosystems even under considerably reduced emission potentials.

As a consequence, simulated global isoprene emissions in R1 (317 $\mathrm{Tg\,yr^{-1}}$) lie at the lower end of the range commonly reported (350 to 800 $\mathrm{Tg\,yr^{-1}}$) in global MEGAN emission studies (Guenther et al., 2012; Messina et al., 2016; Henrot et al., 2017; Sindelarova et al., 2022; Oumami et al., 2024). This difference is obviously primarily linked to the lower emission potentials prescribed in the updated isoprene gridded emission dataset (ε_{ISOP}^{map}), as illustrated by the spatial comparison in Fig. S3, but may also reflect the absence of the CO_2 inhibition (γ_{CO2}) and air quality stress (γ_{AQ}) responses in the present simulations. Nevertheless, the simulated emission ranges in R1 remain consistent with recent studies using MEGAN v3.2, such as Wang et al. (2024) that also reported lower global isoprene emissions (347.7 $\mathrm{Tg\,yr^{-1}}$), or Li et al. which simulated isoprene emissions reduced by a factor 1.7 relative to MEGAN v2.1 over the Qinghai-Tibet Plateau. More generally, the lower emission factors in MEGAN v3.2 are consistent with the recent studies suggesting that MEGAN v2.1 may overestimate isoprene emissions, potentially due to an overestimation of emission potentials for certain vegetation types (Ciarelli et al., 2024).

Despite the overall reduction in annual totals relative to MEGAN v2.1, the seasonal variability of isoprene emissions remains largely preserved. Fig. 4 shows the seasonal global mean emissions for DJF, MAM, JJA, and SON (abbreviations for months from December to November). Maximum emissions occur during boreal summer (JJA), reaching approximately 91 $\mathrm{Tg\,yr^{-1}}$ (Fig. 4.c), reflecting the dominant contribution of Northern Hemisphere vegetation under high-temperature and high-radiation conditions. In contrast, minimum emissions occur during austral summer (69 $\mathrm{Tg\,yr^{-1}}$), despite sustained emissions over tropical regions such as Amazonia and equatorial Africa (Fig. 4.a). This indicates that the MEGAN v3.2 upgrade primarily affects emission magnitudes while preserving the large-scale seasonal dynamics of global isoprene emissions.

https://doi.org/10.5194/egusphere-2026-5773
Preprint. Discussion started: 6 November 2026
© Author(s) 2026. CC BY 4.0 License.

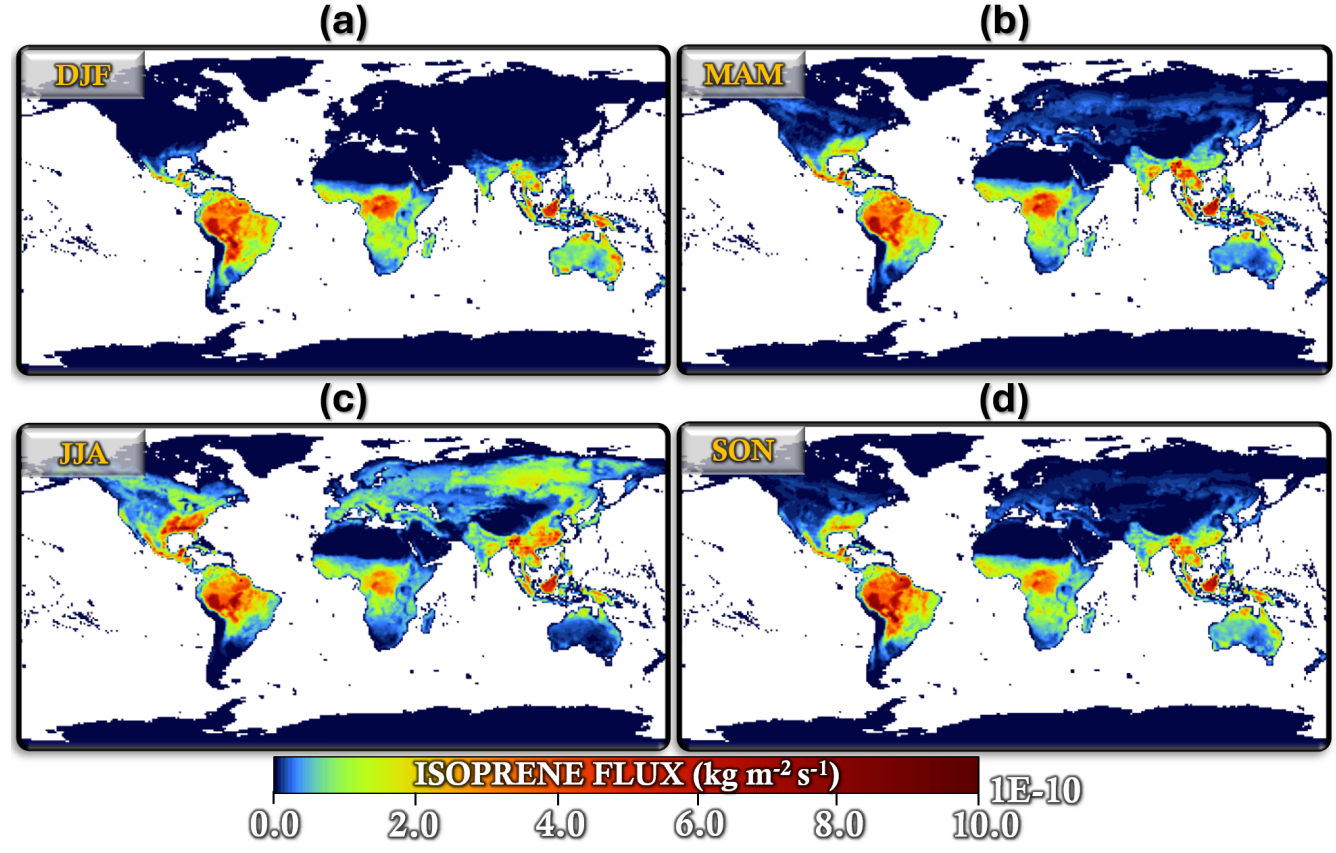


Figure 4. Seasonal spatial distribution of mean isoprene emission in $\mathrm{kg\,m^{-2}\,s^{-1}}$ simulated over 2019 using the R1 simulation during the boreal (a) winter, (b) spring, (c) summer, and (d) autumn.

3.2.2 Sensitivity to soil moisture stress

The impact of the soil moisture activity factor (γ_{SMT}) was evaluated in simulation R2 (Fig. 5). Accounting for soil moisture stress reduces global isoprene emissions by approximately 25.5 % relative to R1, yielding annual totals of 236.7 $\mathrm{Tg\,yr^{-1}}$ (Fig. 5.b). This global reduction is smaller than the -38 % reported by Oumami et al. (2024) for MEGAN v2.1 within SURFEX v8.1, despite the use of an identical γ_{SMT} formulation and a consistent soil-layer configuration between the two model versions. The weaker suppression in MEGAN v3.2 may primarily reflect its lower Baseline isoprene emissions, which results from the reduced emission potentials prescribed in the update ε^{map}_{ISOP} dataset (Sect. 3.2.1). Consequently, reductions in emissions potentials probably indirectly mitigate the absolute contribution of drought stress to the global isoprene budget.

The annual mean spatial distribution of γ_{SMT} simulated in R2 is presented in Fig. S4. Values close to zero indicate strong soil moisture stress suppressing isoprene emission fluxes, whereas values close to one indicate minimal moisture limitation. The spatial pattern reveals a pronounced regional contrast. Over most of North America, Europe, and Amazonia, γ_{SMT} remains close to one throughout the year, reflecting persistently high soil moisture availability and limited impacts on isoprene emissions

https://doi.org/10.5194/egusphere-2026-5773
Preprint. Discussion started: 6 November 2026
© Author(s) 2026. CC BY 4.0 License.

in these regions. By contrast, strong suppression is simulated over south-eastern Australia, southern Africa (Namibia), Chile, and parts of the Indian sub-continent, where γ_{SMT} approaches zero in response to recurrent seasonal drought conditions characteristics of semi-arid and arid environments.

These spatial patterns are directly reflected in regional emission response (Table S2). Relative to R1, the largest reductions are simulated over Australia (-73.1 %) and southern Africa (-60.8 %), highlighting the dominant role of drought stress in constraining BVOC emissions over water-limited ecosystems. These results are consistent with previous studies reporting strong reductions in isoprene emissions under drought conditions, particularly in semi-arid ecosystems (Emmerson et al., 2019; Opacka et al., 2022; Strada et al., 2023). Consequently, the activation of γ_{SMT} induces considerably larger changes in global emission totals, emphasizing the importance of accurately representing drought stress in BVOC emission models (Wang et al., 2022).

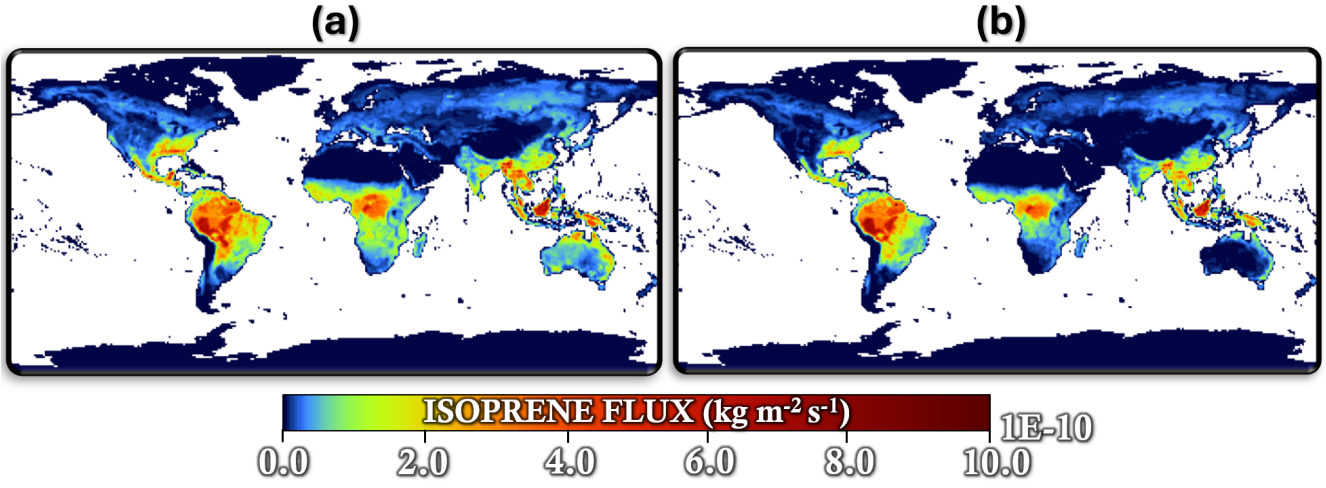


Figure 5. Spatial distribution of annual mean isoprene emission fluxes ($\mathrm{kg\,m^{-2}\,s^{-1}}$) simulated for 2019 using ERA5 reanalyses and conducted with (a) R1 and (b) R2 simulations, i.e. with γ_{SMT} turned off and on respectively.

The seasonal structure of isoprene emissions (Table S3) remains largely preserved under soil moisture stress, with JJA remaining the season of maximum global emissions (70.2 $\mathrm{Tg\,yr^{-1}}$) and DJF the minimum (53.5 $\mathrm{Tg\,yr^{-1}}$). However, the relative suppression varies seasonally, ranging from -22.9 % in JJA to -28.9 % in SON. Indeed, the weaker suppression during boreal summer probably reflects the dominant contribution of productive but moderately moist Northern Hemisphere ecosystems (Europe, North America) which drive summer emissions but experience limited drought stress, while the stronger suppression in SON may reflect enhanced soil moisture limitation following austral summer drying (Australia and southern Africa). Overall, soil moisture stress significantly reduces the magnitude of global isoprene emissions while largely preserving the seasonality of the annual isoprene emission cycle.

Yet, the effective impacts of soil moisture on isoprene emissions remain highly uncertain, particularly regarding its representation in emission models, and continues to be an active area of research (Jiang et al., 2018; Bonn et al., 2019). Furthermore,

https://doi.org/10.5194/egusphere-2026-5773
Preprint. Discussion started: 6 November 2026
© Author(s) 2026. CC BY 4.0 License.

some studies, still neglect in particular soil moisture effects entirely in MEGAN simulations (Sindelarova et al., 2022; Oomen et al., 2024). Consequently, soil moisture stress is deactivated in the subsequent sensitivity experiments R3 and R4 (Sect. 3.2.3), which should in addition isolate the respective contributions of emission factor parametrization and land-cover description independently of the drought stress effects quantified in this section.

3.2.3 Impacts of PFT-dependent emission factors

Additional sensitivity experiments were conducted to evaluate the effects of reintroducing PFT-dependent emission factors ($\varepsilon_{k,i}$) and updating the land cover database in MEGAN v3.2.

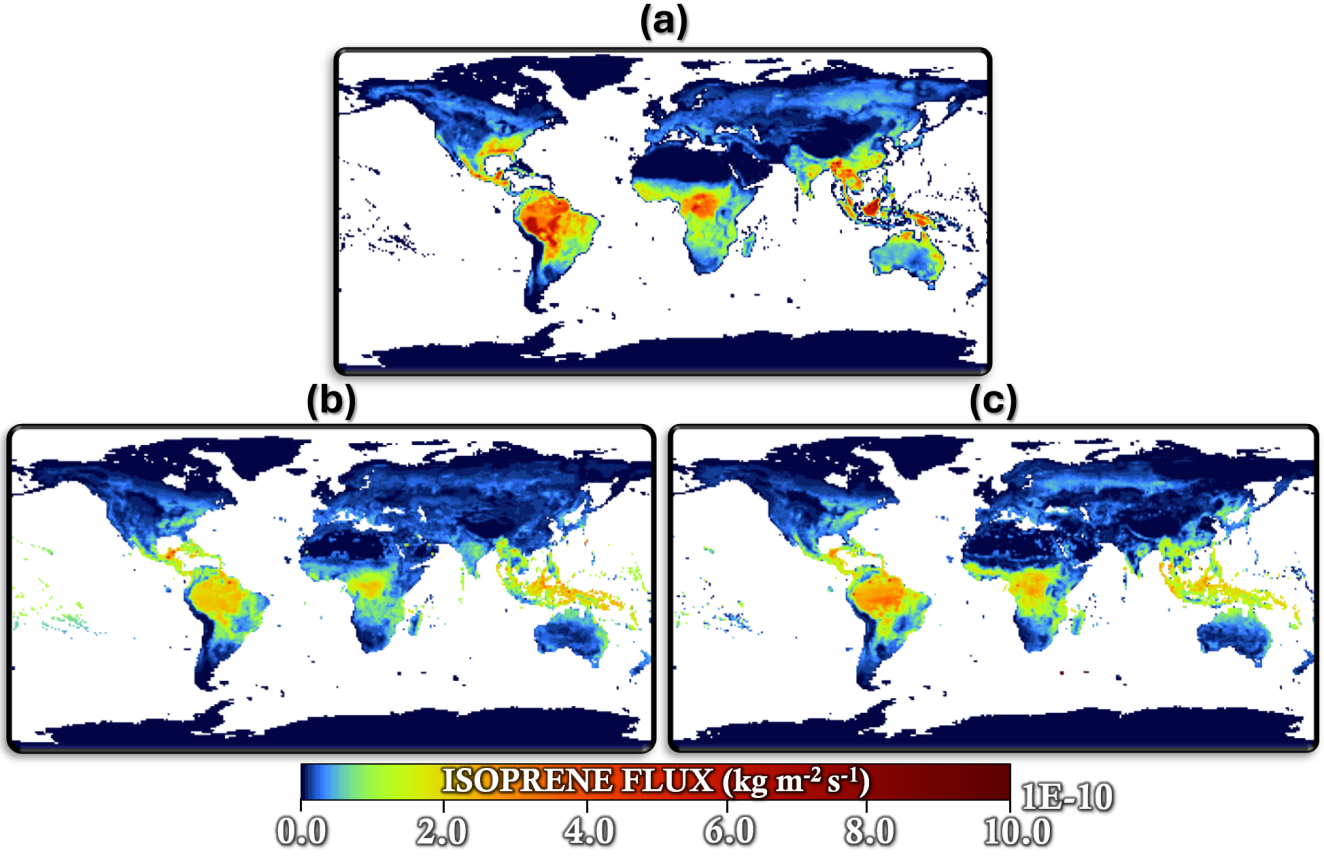


Figure 6. Spatial distribution of annual mean isoprene emission fluxes ($\mathrm{kg\,m^{-2}\,s^{-1}}$) simulated for 2019 using ERA5 reanalyses and conducted with (a) R1 and (b,c) R3 simulations, i.e. with $\varepsilon_{k,i}$ reintroduced and employed in panel (b,c) rather than ε_i^{map} (a). A sensitivity test using (b) ECOCLIMAP-I and (c) ECOCLIMAP-SG land-cover datasets is also simulated.

Figure 6.b first presents global isoprene emissions simulated in experiment R3, in which PFT-dependent emission potentials ($\varepsilon_{k,ISOP}$) replace the gridded emission potential maps (ε_{ISOP}^{map}, Fig.6.a) used to compute emission factors. Consistent with findings reported in MEGAN v2.1 by Oumami et al. (2024), the use of $\varepsilon_{k,ISOP}$ yields lower global isoprene emissions than

https://doi.org/10.5194/egusphere-2026-5773
Preprint. Discussion started: 6 November 2026
© Author(s) 2026. CC BY 4.0 License.

ε_{ISOP}^{map}-based simulations, with annual totals of 240.0 $\mathrm{Tg\,yr^{-1}}$ (Fig. 6.b), representing a 24.4 % global annual emission decrease relative to R1 (Fig.6.a). However, this sensitivity to emission factor parametrization is considerably amplified in MEGAN v3.2 (i.e. twice as large compared to MEGAN v2.1 as reported in Oumami et al. (2024)), reflecting the larger divergence between the upgraded gridded ε_{ISOP}^{map} dataset and the prescribed PFT-dependent $\varepsilon_{k,ISOP}$ values implemented in MEGAN v3.2. In addition, beyond reducing annual totals, the use of $\varepsilon_{k,ISOP}$ seems to decrease mean daily emissions (approximately 0.65 $\mathrm{Tg\,day^{-1}}$ in R3 versus 0.83 $\mathrm{Tg\,day^{-1}}$ in R1) and dampens the amplitude of the boreal summer emission peak, resulting in a weaker seasonal cycle overall (Fig. S5). Nonetheless, the re-implementation of ε_i^{map} in MEGAN v3.2 provides a useful and promising framework for future climate simulations involving dynamics vegetation variables.

The reintroduction of $\varepsilon_{k,i}$ also enabled the evaluation of the ECOCLIMAP-SG land-cover database in experiment R4 (Fig. 6.c). Compared with ECOCLIMAP-I (Fig.6.b), ECOCLIMAP-SG produces higher global isoprene emissions, with annual totals increasing by approximately 9 %, reaching 261.5 $\mathrm{Tg\,yr^{-1}}$ (Fig. 6.c). Furthermore, the comparison of PFT-dependent isoprene emission potentials between the two land-cover databases reveals a broadly similar spatial structure (Pearson r = 0.84), indicating that the two datasets assign emission potentials to the same geographical regions, although with systematically higher values in ECOCLIMAP-SG. Yet, as shown in the spatial difference maps (Fig. S6), the transition from ECOCLIMAP-I to ECOCLIMAP-SG induces a complex regional redistribution of isoprene emissions rather than a uniform global increase. The largest positive contributions come from East Africa (26.30 %), Australia (20.70 %), and Southeast Asia (13.60 %), consistent with a higher fraction of tropical forest PFTs (which carry high isoprene emission potentials) in ECOCLIMAP-SG over these regions. Overall, the Southern Hemisphere (+15.1 %) shows a larger response than the Northern Hemisphere (+4.5 %), consistent with the dominant contribution of these regions to the global emission increase.

In the end, the combination of ECOCLIMAP-SG and PFT-dependent emission factors ($\varepsilon_{k,i}$) appears particularly promising for future applications involving dynamic vegetation variables such as LAI and PFT distributions, with annual isoprene estimates reaching 262 $\mathrm{Tg\,yr^{-1}}$.

3.2.4 Sensitivity to meteorological forcing datasets

All experiments presented in the previous sections were finally performed using both ERA5 reanalysis and IFS (Integrated Forecasting System) forecast meteorological forcing, allowing a systematic assessment of how the sensitivity of simulated isoprene emissions to meteorological forcing evolves across the different model configurations tested in this study. Figure 7 provides a synthetic overview of this assessment, showing daily differences in global isoprene emissions for each of the five developments evaluated above (Sect. 3). Each panel displays four quantities computed from two pairs of simulations: the ERA5-IFS daily difference before (light blue solid line) and after (dark blue solid line) the development, and the impact of the development under ERA5 (dark orange dashed line) and IFS (light orange dashed line) forcing. The blue shaded area between the two lines characterises whether the development amplifies or reduces the ERA5-IFS spread, while the orange shaded area defines whether the development impact is consistent across forcing.

A first key result concerns the evolution of the ERA5-IFS forcing uncertainty (blue shaded area) across developments. Specifically, in most configurations, the ERA5-IFS spread remains of comparable magnitude, indicating that the model de-

https://doi.org/10.5194/egusphere-2026-5773
Preprint. Discussion started: 6 November 2026
© Author(s) 2026. CC BY 4.0 License.

velopments tested here do not fundamentally alter the sensitivity of simulated isoprene emissions to meteorological forcing. Hence, each source of uncertainty can be assessed independently of the others. Yet, a slightly reduced ERA5-IFS spread is noticeable when soil moisture stress is activated (Fig. 7.c), suggesting that both forcing produce similar soil moisture stress patterns that dampen forcing differences, an expected behaviour given that soil moisture stress is primarily driven by SURFEX land surface variables rather than by the atmospheric forcing fields directly. A second key result is that across all panels, the amplitude of the orange lines (development sensitivity) consistently exceeds that of the blue lines (forcing uncertainty), confirming that the MEGAN v3.2 upgrade (Fig. 7.b), soil moisture stress (Fig. 7.c), emission factor parametrization (Fig. 7.d), and land-cover description (Fig. 7.e) each constitute a larger source of uncertainty in simulated isoprene budgets than the choice between ERA5 and IFS forcing. This characteristic is likely robust throughout the year and is not confined to a particular season.

Examining the global annual totals across experiments, IFS forcing systematically produces lower isoprene emissions than ERA5 across all ECOCLIMAP-I-based simulations (Fig. 7.a-d), with especially a discrepancy of approximately 5 % in MEGAN v2.1 (Oumami et al., 2024) that increases to about 10 % in R1 (Fig. 7.b). This suggests that the updated MEGAN v3.2 parametrization amplifies rather than reduces the sensitivity to meteorological forcing uncertainty. This amplification is consistent with a stronger non-linear response of the new activity factors or emission factor dataset to the meteorological differences between ERA5 and IFS. Despite this, the ERA5-IFS spread remains comparatively small regardless of the emission factor approach (R3, Fig. 7.d), confirming that uncertainties associated with emission factor parametrization exceed those related to meteorological forcing in the present framework.

One notable exception concerns the SURFEX upgrade (Fig. 7.a), where the forcing uncertainty is of comparable magnitude (and in the IFS case even larger than) to the development sensitivity itself. As discussed in Section 3.1, the SURFEX upgrade produces a global emission reduction of -4.1 % under ERA5, but -12 % here under IFS, likely reflecting the greater spatial heterogeneity of IFS forecast fields compared to ERA5 reanalysis fields, which amplifies the response to the updated processing schemes in SURFEX v9.0. However, given the limited overall global impact of the SURFEX upgrade, this exception does not affect the conclusions drawn from subsequent experiments.

A second exception concerns the ECOCLIMAP-SG sensitivity test (Fig. 7.e), where the orange shaded area is considerably wider than in other panels, and where the ERA5-IFS emission ordering is reversed relative to all other configurations. Precisely, IFS yields high global isoprene emissions than ERA5 in R4 (290.3 vs 261.5 $\mathrm{Tg\,yr^{-1}}$), with the contrast driven entirely by the Southern Hemisphere (Table S4), where IFS produces 24.3 % higher emissions than ERA5 (161.6 vs 130.0 $\mathrm{Tg\,yr^{-1}}$) while the Northern Hemisphere shows a negligible difference (-2.1 %). Since soil moisture stress is deactivated in R4, this reversal likely reflects temperature and radiation contrast between the two forcing amplified by the model land surface characteristics of ECOCLIMAP-SG, particularly over the Southern Hemisphere, and is associated with a significant reorganisation of the geographical distribution of isoprene hotspots (Pearson r = 0.75, Table S4). This finding demonstrates that the sensitivity of simulated isoprene emissions to meteorological forcing is not an intrinsic property of the forcing datasets alone but also depends critically on the land surface representation used in the model.

https://doi.org/10.5194/egusphere-2026-5773
Preprint. Discussion started: 6 November 2026
© Author(s) 2026. CC BY 4.0 License.

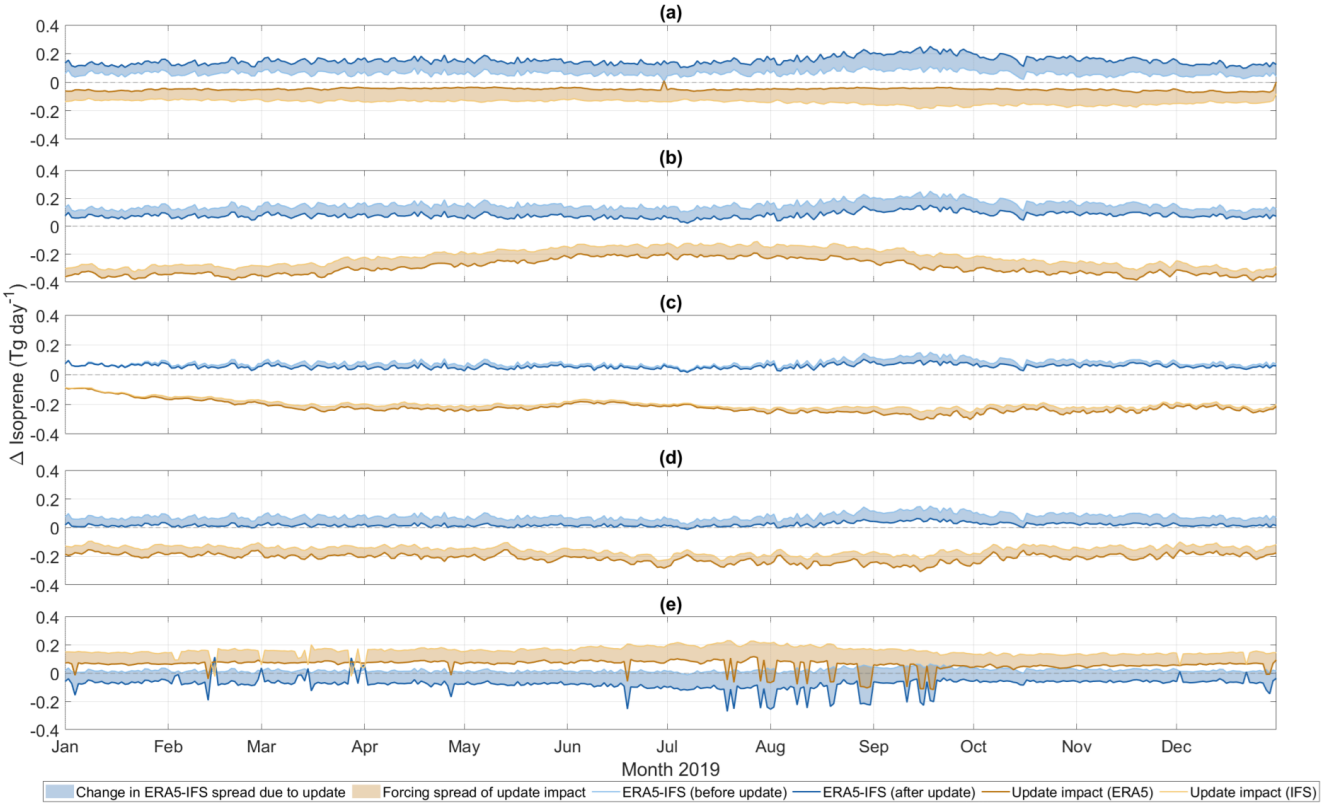


Figure 7. Daily sensitivity of global isoprene emissions ($\mathrm{Tg\,day^{-1}}$) to meteorological forcing and model developments throughout 2019. Each panel corresponds to one development tested: (a) SURFEX upgrade, (b) MEGAN v3.2 upgrade, (c) soil moisture stress (γ_{SMT}), (d) emission factor approach (ε_i^{map} vs $\varepsilon_{k,i}$), and (e) land-cover database (ECOCLIMAP-I vs ECOCLIMAP-SG). In each panel, the light and dark blue solid lines represent the ERA5-IFS daily emission difference before and after the development respectively, with the blue shaded area highlighting the change in forcing uncertainty induced by the development. The dark and light orange dashed lines represent the daily emission difference attributable to the development under ERA5 and IFS forcing respectively, with the orange shaded area representing the spread of the development sensitivity across forcing.

Taken together, these results confirm that choices of emission factor parametrizations and land-cover descriptions are the leading sources of uncertainty in simulated global isoprene budgets within the SURFEX-MEGAN framework, with meteorological forcing representing a secondary but non-negligible source of uncertainty whose magnitude and sign depend on the model configuration.

4 Conclusions

The present study implements and evaluates the latest version of the MEGAN biogenic emission model (MEGAN v3.2) within SURFEX v9.0, following the coupling framework previously developed by Oumami et al. (2024). A series of global

https://doi.org/10.5194/egusphere-2026-5773
Preprint. Discussion started: 6 November 2026
© Author(s) 2026. CC BY 4.0 License.

offline simulations was performed aiming to assess the impacts of the MEGAN upgrade, soil moisture stress, emission factor parametrization, and land-cover description on simulated BVOC emissions, with a particular focus on isoprene.

The upgrade of SURFEX from v8.1 to v9.0 was first evaluated in combination with MEGAN v2.1 and was found to have no significant impact on simulated isoprene emissions, confirming that the land surface upgrade does not introduce unintended biases in the natural-tile physics relevant to biogenic emissions. The subsequent transition from MEGAN v2.1 to MEGAN v3.2 leads to considerably lower global isoprene emissions, with simulated annual totals ranging from 216 to 318 $\mathrm{Tg\,yr^{-1}}$ depending on the meteorological forcing and activity factors considered, values at the lower end of the range commonly reported in global MEGAN studies. This reduction is primarily attributable to the updated gridded emission factor dataset in MEGAN v3.2, which introduces significantly lower emission potentials across most land regions, particularly in the Southern Hemisphere, which contributes nearly to 65 % of the global emission decrease albeit representing only 22 % of vegetated land grid cells. Despite the hemispheric asymmetry in magnitude, the high spatial Pearson correlation between versions (r = 0.93) confirms that the upgrade primarily rescales emission intensities rather than fundamentally reorganizing the geographical distribution of emission hotspots. The lower emissions simulated with MEGAN v3.2 are nevertheless broadly consistent with recent studies suggesting that MEGAN v2.1 may overestimate isoprene emission potentials for some vegetation types (Ciarelli et al., 2024), and the large-scale seasonal structure of emissions remains largely preserved.

Sensitivity experiments further demonstrate the major role of environmental stress and land surface representation in controlling BVOC emissions. The activation of soil moisture stress reduces global isoprene emissions by approximately 26 %, with the strongest suppression occurring over semi-arid and drought-prone ecosystems such as Australia and southern Africa, while largely preserving the seasonality of the annual emission cycle. Additional experiments using PFT-dependent emission factors and the ECOCLIMAP-SG land-cover database further demonstrate that emission factor parametrization and land-cover representation constitute first-order controls on simulated BVOC emissions, with associated uncertainties exceeding those related to meteorological forcing. In particular, the use of ECOCLIMAP-SG reverses the ERA5-IFS emission ordering observed in all other simulations, driven by a forcing-dependent amplification of surface energy balance differences. This reversal is accompanied by a substantial spatial reorganization of emission hotspots (Pearson r = 0.75 in the Southern Hemisphere between ERA5 and IFS using ECOCLIMAP-SG land-cover dataset), revealing a strong non-linear interaction between land surface characterization and meteorological forcing that warrants further investigation.

Overall, these developments considerably improve the flexibility and realism of the SURFEX-MEGAN framework for global BVOC simulations. The implementation of MEGAN v3.2 within SURFEX v9.0 provides a robust basis for future applications, notably involving dynamic vegetation, evolving land-cover distributions, and coupled-chemistry-climate interactions. Future work should among other 1) investigate the impact of the CO_2 inhibition and air quality stress responses (currently deactivated in this study), along with 2) perform comparisons against other biogenic emission models, as well as 3) evaluate the framework in fully coupled atmospheric chemistry simulations.

https://doi.org/10.5194/egusphere-2026-5773
Preprint. Discussion started: 6 November 2026
© Author(s) 2026. CC BY 4.0 License.

Code availability. The SURFEX-MEGAN coupled framework developed in this study (Salignat et al., 2026a) is available at https://doi.org/10.5281/zenodo.21698653.

Data availability. The physiographic input fields used in this study are available at https://doi.org/10.5281/zenodo.21699036 (Salignat et al., 2026b). ERA5 meteorological fields are available from the Copernicus Climate Data Store at https://doi.org/10.24381/cds.adbb2d47 (Hersbach et al., 2023a, b). IFS forecast fields are available to the ECMWF (European Center for Medium-Range Weather Forecasts) members, the members "can not redistribute, sell, broker or licence the valid products to any third party". The simulation outputs produced in this study are available at https://doi.org/10.5281/zenodo.21699207 (Salignat et al., 2026c).

Author contributions. RS performed the modifications applied to the new coupled SURFEX-MEGAN framework, ran all model simulations, analyzed the results, and led the writing of the manuscript. RS and JAm generated the gridded emission factor datasets. JAr supervised the project. All co-authors contributed to the scientific discussion and to reviewing and editing the manuscript.

Competing interests. The authors declare that they have no conflict of interest

Acknowledgements. This work has beneficied from state aid managed by the National Research Agency under France 2030 as part of the PEPR TRACCS programme under grant number ANR-22-EXTR-0009 (TRACCS-PC8-CYCL-ESM project).

https://doi.org/10.5194/egusphere-2026-5773
Preprint. Discussion started: 6 November 2026
© Author(s) 2026. CC BY 4.0 License.

References

Arneth, A., Schurgers, G., Lathiere, J., Duhl, T., Beerling, D. J., Hewitt, C. N., Martin, M., and Guenther, A.: Global terrestrial isoprene emission models: sensitivity to variability in climate and vegetation, Atmospheric Chemistry and Physics, 11, 8037–8052, https://doi.org/10.5194/acp-11-8037-2011, 2011.

Bettineschi, M., Cholakian, A., Sinclair, V., Sindelarova, K., Praplan, A. P., Thomas, S. J., Petäjä, T., Bianchi, F., and Ciarelli, G.: Improved isoprene emission estimates over the Finnish boreal forest using the MEGANv3.2 model, Atmospheric Chemistry and Physics, 26, 8067–8088, https://doi.org/10.5194/acp-26-8067-2026, 2026.

Bonn, B., Magh, R.-K., Rombach, J., and Kreuzwieser, J.: Biogenic isoprenoid emissions under drought stress: different responses for isoprene and terpenes, Biogeosciences, 16, 4627–4645, https://doi.org/10.5194/bg-16-4627-2019, 2019.

Calvet, J.-C., Noilhan, J., Roujean, J.-L., Bessemoulin, P., Cabelguenne, M., Olioso, A., and Wigneron, J.-P.: An interactive vegetation SVAT model tested against data from six contrasting sites, Agricultural and Forest Meteorology, 92, 73–95, https://doi.org/10.1016/s0168-1923(98)00091-4, 1998.

Carlton, A. G., Wiedinmyer, C., and Kroll, J. H.: A review of Secondary Organic Aerosol (SOA) formation from isoprene, Atmospheric Chemistry and Physics, 9, 4987–5005, https://doi.org/10.5194/acp-9-4987-2009, 2009.

Carslaw, K. S., Boucher, O., Spracklen, D. V., Mann, G. W., Rae, J. G. L., Woodward, S., and Kulmala, M.: A review of natural aerosol interactions and feedbacks within the Earth system, Atmospheric Chemistry and Physics, 10, 1701–1737, https://doi.org/10.5194/acp-10-1701-2010, 2010.

Cholakian, A., Beekmann, M., Siour, G., Coll, I., Cirtog, M., Ormeño, E., Flaud, P.-M., Perraudin, E., and Villenave, E.: Simulation of organic aerosol, its precursors, and related oxidants in the Landes pine forest in southwestern France: accounting for domain-specific land use and physical conditions, Atmospheric Chemistry and Physics, 23, 3679–3706, https://doi.org/10.5194/acp-23-3679-2023, 2023.

Ciarelli, G., Tahvonen, S., Cholakian, A., Bettineschi, M., Vitali, B., Petäjä, T., and Bianchi, F.: On the formation of biogenic secondary organic aerosol in chemical transport models: an evaluation of the WRF-CHIMERE (v2020r2) model with a focus over the Finnish boreal forest, Geoscientific Model Development, 17, 545–565, https://doi.org/10.5194/gmd-17-545-2024, 2024.

Dreyfus, G. B., Schade, G. W., and Goldstein, A. H.: Observational constraints on the contribution of isoprene oxidation to ozone production on the western slope of the Sierra Nevada, California, Journal of Geophysical Research: Atmospheres, 107, https://doi.org/10.1029/2001jd001490, 2002.

Druel, A., Munier, S., Mucia, A., Albergel, C., and Calvet, J.-C.: Implementation of a new crop phenology and irrigation scheme in the ISBA land surface model using SURFEX v8.1, Geoscientific Model Development, 15, 8453–8471, https://doi.org/10.5194/gmd-15-8453-2022, 2022.

Emmerson, K. M., Palmer, P. I., Thatcher, M., Haverd, V., and Guenther, A. B.: Sensitivity of isoprene emissions to drought over south-eastern Australia: Integrating models and satellite observations of soil moisture, Atmospheric Environment, 209, 112–124, https://doi.org/10.1016/j.atmosenv.2019.04.038, 2019.

Faroux, S., Kaptué Tchuenté, A. T., Roujean, J.-L., Masson, V., Martin, E., and Le Moigne, P.: ECOCLIMAP-II/Europe: a twofold database of ecosystems and surface parameters at 1 km resolution based on satellite information for use in land surface, meteorological and climate models, Geoscientific Model Development, 6, 563–582, https://doi.org/10.5194/gmd-6-563-2013, 2013.

https://doi.org/10.5194/egusphere-2026-5773
Preprint. Discussion started: 6 November 2026
© Author(s) 2026. CC BY 4.0 License.

Guenther, A., Hewitt, C. N., Erickson, D., Fall, R., Geron, C., Graedel, T., Harley, P., Klinger, L., Lerdau, M., Mckay, W. A., Pierce, T., Scholes, B., Steinbrecher, R., Tallamraju, R., Taylor, J., and Zimmerman, P.: A global model of natural volatile organic compound emissions, Journal of Geophysical Research: Atmospheres, 100, 8873–8892, https://doi.org/10.1029/94jd02950, 1995.

Guenther, A., Karl, T., Harley, P., Wiedinmyer, C., Palmer, P. I., and Geron, C.: Estimates of global terrestrial isoprene emissions using MEGAN (Model of Emissions of Gases and Aerosols from Nature), Atmospheric Chemistry and Physics, 6, 3181–3210, https://doi.org/10.5194/acp-6-3181-2006, 2006.

Guenther, A., Jiang, X., Shah, T., Huang, L., Kemball-Cook, S., and Yarwood, G.: Model of Emissions of Gases and Aerosol from Nature Version 3 (MEGAN3) for Estimating Biogenic Emissions, p. 187–192, Springer International Publishing, ISBN 9783030220556, https://doi.org/10.1007/978-3-030-22055-6_29, 2019.

Guenther, A. B., Monson, R. K., and Fall, R.: Isoprene and monoterpene emission rate variability: Observations with eucalyptus and emission rate algorithm development, Journal of Geophysical Research: Atmospheres, 96, 10 799–10 808, https://doi.org/10.1029/91jd00960, 1991.

Guenther, A. B., Zimmerman, P. R., Harley, P. C., Monson, R. K., and Fall, R.: Isoprene and monoterpene emission rate variability: Model evaluations and sensitivity analyses, Journal of Geophysical Research: Atmospheres, 98, 12 609–12 617, https://doi.org/10.1029/93jd00527, 1993.

Guenther, A. B., Jiang, X., Heald, C. L., Sakulyanontvittaya, T., Duhl, T., Emmons, L. K., and Wang, X.: The Model of Emissions of Gases and Aerosols from Nature version 2.1 (MEGAN2.1): an extended and updated framework for modeling biogenic emissions, Geoscientific Model Development, 5, 1471–1492, https://doi.org/10.5194/gmd-5-1471-2012, 2012.

Guo, H., Ling, Z. H., Simpson, I. J., Blake, D. R., and Wang, D. W.: Observations of isoprene, methacrolein (MAC) and methyl vinyl ketone (MVK) at a mountain site in Hong Kong, Journal of Geophysical Research: Atmospheres, 117, https://doi.org/10.1029/2012jd017750, 2012.

Hallquist, M., Wenger, J. C., Baltensperger, U., Rudich, Y., Simpson, D., Claeys, M., Dommen, J., Donahue, N. M., George, C., Goldstein, A. H., Hamilton, J. F., Herrmann, H., Hoffmann, T., Iinuma, Y., Jang, M., Jenkin, M. E., Jimenez, J. L., Kiendler-Scharr, A., Maenhaut, W., McFiggans, G., Mentel, T. F., Monod, A., Prévôt, A. S. H., Seinfeld, J. H., Surratt, J. D., Szmigielski, R., and Wildt, J.: The formation, properties and impact of secondary organic aerosol: current and emerging issues, Atmospheric Chemistry and Physics, 9, 5155–5236, https://doi.org/10.5194/acp-9-5155-2009, 2009.

Hamer, P. D., Markelj, M., Rojas-Munoz, O., Bonan, B., Calvet, J.-C., Marécal, V., Guenther, A., Trimmel, H., Vallejo, I., Eckhardt, S., Sousa Santos, G., Sindelarova, K., Simpson, D., Schmidbauer, N., Hellén, H., Rubli, P., Reimann, S., Claude, A., Kubistin, D., Cozic, J., Dernie, J., and Tarrasón, L.: Two biogenic volatile organic compound emission datasets over Europe based on land surface modelling and satellite data assimilation, Earth System Science Data, 18, 3635–3669, https://doi.org/10.5194/essd-18-3635-2026, 2026.

Harrison, S. P., Morfopoulos, C., Dani, K. G. S., Prentice, I. C., Arneth, A., Atwell, B. J., Barkley, M. P., Leishman, M. R., Loreto, F., Medlyn, B. E., Niinemets, U., Possell, M., Peñuelas, J., and Wright, I. J.: Volatile isoprenoid emissions from plastid to planet, New Phytologist, 197, 49–57, https://doi.org/10.1111/nph.12021, 2012.

Heald, C. L., Wilkinson, M. J., Monson, R. K., Alo, C. A., Wang, G., and Guenther, A.: Response of isoprene emission to ambient CO₂ changes and implications for global budgets, Global Change Biology, 15, 1127–1140, https://doi.org/10.1111/j.1365-2486.2008.01802.x, 2009.

Henrot, A.-J., Stanelle, T., Schröder, S., Siegenthaler, C., Taraborrelli, D., and Schultz, M. G.: Implementation of the MEGAN (v2.1) biogenic emission model in the ECHAM6-HAMMOZ chemistry climate model, Geoscientific Model Development, 10, 903–926, https://doi.org/10.5194/gmd-10-903-2017, 2017.

https://doi.org/10.5194/egusphere-2026-5773
Preprint. Discussion started: 6 November 2026
© Author(s) 2026. CC BY 4.0 License.

Hersbach, H., Bell, B., Berrisford, P., Biavati, G., Horáanyi, A., Muñoz Sabater, J., Nicolas, J., Peubey, C., Radu, R., Rozum, I., Schepers, D., Simmons, A., Soci, C., Dee, D., and Thépaut, J. N.: ERA5 hourly data on pressure levels from 1940 to present, https://doi.org/10.24381/CDS.BD0915C6, 2023a.

Hersbach, H., Bell, B., Berrisford, P., Biavati, G., Horányi, A., Muñoz Sabater, J., Nicolas, J., Peubey, C., Radu, R., Rozum, I., Schepers, D., Simmons, A., Soci, C., Dee, D., and Théepaut, J. N.: ERA5 hourly data on single levels from 1940 to present, https://doi.org/10.24381/CDS.ADBB2D47, 2023b.

IPCC: Climate Change 2021 – The Physical Science Basis: Working Group I Contribution to the Sixth Assessment Report of the Intergovernmental Panel on Climate Change, Cambridge University Press, ISBN 9781009157896, https://doi.org/10.1017/9781009157896, 2021.

Jiang, J., Aksoyoglu, S., Ciarelli, G., Oikonomakis, E., El-Haddad, I., Canonaco, F., O'Dowd, C., Ovadnevaite, J., Minguillón, M. C., Baltensperger, U., and Prévôt, A. S. H.: Effects of two different biogenic emission models on modelled ozone and aerosol concentrations in Europe, Atmospheric Chemistry and Physics, 19, 3747–3768, https://doi.org/10.5194/acp-19-3747-2019, 2019.

Jiang, X., Guenther, A., Potosnak, M., Geron, C., Seco, R., Karl, T., Kim, S., Gu, L., and Pallardy, S.: Isoprene emission response to drought and the impact on global atmospheric chemistry, Atmospheric Environment, 183, 69–83, https://doi.org/10.1016/j.atmosenv.2018.01.026, 2018.

Lathière, J., Hauglustaine, D. A., Friend, A. D., De Noblet-Ducoudré, N., Viovy, N., and Folberth, G. A.: Impact of climate variability and land use changes on global biogenic volatile organic compound emissions, Atmospheric Chemistry and Physics, 6, 2129–2146, https://doi.org/10.5194/acp-6-2129-2006, 2006.

Le Moigne, P.: SURFEX scientific documentation, V8.1, http://www.umr-cnrm.fr/surfex/IMG/pdf/surfex_scidoc_v8.1.pdf, last access: 27 May 2026, 2018.

Li, P., Yu, Y., and Zhao, S.: Comparative assessment of MEGAN v2.1 and v3.2 biogenic VOC emissions over the Qinghai-Tibet Plateau: implications for summertime surface ozone simulations, in revision.

Messina, P., Lathière, J., Sindelarova, K., Vuichard, N., Granier, C., Ghattas, J., Cozic, A., and Hauglustaine, D. A.: Global biogenic volatile organic compound emissions in the ORCHIDEE and MEGAN models and sensitivity to key parameters, Atmospheric Chemistry and Physics, 16, 14 169–14 202, https://doi.org/10.5194/acp-16-14169-2016, 2016.

Müller, J.-F., Stavrakou, T., Wallens, S., De Smedt, I., Van Roozendael, M., Potosnak, M. J., Rinne, J., Munger, B., Goldstein, A., and Guenther, A. B.: Global isoprene emissions estimated using MEGAN, ECMWF analyses and a detailed canopy environment model, Atmospheric Chemistry and Physics, 8, 1329–1341, https://doi.org/10.5194/acp-8-1329-2008, 2008.

Munier, S., Carrer, D., Planque, C., Camacho, F., Albergel, C., and Calvet, J.-C.: Satellite Leaf Area Index: Global Scale Analysis of the Tendencies Per Vegetation Type Over the Last 17 Years, Remote Sensing, 10, 424, https://doi.org/10.3390/rs10030424, 2018.

Noilhan, J. and Planton, S.: A Simple Parameterization of Land Surface Processes for Meteorological Models, Monthly Weather Review, 117, 536–549, https://doi.org/10.1175/1520-0493(1989)117<0536:aspols>2.0.co;2, 1989.

Oomen, G.-M., Müller, J.-F., Stavrakou, T., De Smedt, I., Blumenstock, T., Kivi, R., Makarova, M., Palm, M., Röhling, A., Té, Y., Vigouroux, C., Friedrich, M. M., Frieß, U., Hendrick, F., Merlaud, A., Piters, A., Richter, A., Van Roozendael, M., and Wagner, T.: Weekly derived top-down volatile-organic-compound fluxes over Europe from TROPOMI HCHO data from 2018 to 2021, Atmospheric Chemistry and Physics, 24, 449–474, https://doi.org/10.5194/acp-24-449-2024, 2024.

https://doi.org/10.5194/egusphere-2026-5773
Preprint. Discussion started: 6 November 2026
© Author(s) 2026. CC BY 4.0 License.

Opacka, B., Müller, J.-F., Stavrakou, T., Miralles, D. G., Koppa, A., Pagán, B. R., Potosnak, M. J., Seco, R., De Smedt, I., and Guenther, A. B.: Impact of Drought on Isoprene Fluxes Assessed Using Field Data, Satellite-Based GLEAM Soil Moisture and HCHO Observations from OMI, Remote Sensing, 14, 2021, https://doi.org/10.3390/rs14092021, 2022.

Oumami, S., Arteta, J., Guidard, V., Tulet, P., and Hamer, P. D.: Evaluation of isoprene emissions from the coupled model SURFEX–MEGANv2.1, Geoscientific Model Development, 17, 3385–3408, https://doi.org/10.5194/gmd-17-3385-2024, 2024.

Pacifico, F., Folberth, G. A., Jones, C. D., Harrison, S. P., and Collins, W. J.: Sensitivity of biogenic isoprene emissions to past, present, and future environmental conditions and implications for atmospheric chemistry, Journal of Geophysical Research: Atmospheres, 117, https://doi.org/10.1029/2012jd018276, 2012.

Palmer, P. I., Abbot, D. S., Fu, T., Jacob, D. J., Chance, K., Kurosu, T. P., Guenther, A., Wiedinmyer, C., Stanton, J. C., Pilling, M. J., Pressley, S. N., Lamb, B., and Sumner, A. L.: Quantifying the seasonal and interannual variability of North American isoprene emissions using satellite observations of the formaldehyde column, Journal of Geophysical Research: Atmospheres, 111, https://doi.org/10.1029/2005jd006689, 2006.

Peñuelas, J. and Staudt, M.: BVOCs and global change, Trends in Plant Science, 15, 133–144, https://doi.org/10.1016/j.tplants.2009.12.005, 2010.

Riches, M., Snook, J., and Farmer, D. K.: The First Seasonal Snowfall Impacts Plant Photosynthesis and Monoterpene Emissions, Geophysical Research Letters, 49, https://doi.org/10.1029/2022gl100368, 2022.

Rinne, H., Guenther, A., Greenberg, J., and Harley, P.: Isoprene and monoterpene fluxes measured above Amazonian rainforest and their dependence on light and temperature, Atmospheric Environment, 36, 2421–2426, https://doi.org/10.1016/s1352-2310(01)00523-4, 2002.

Rocco, M., Brugere, E., Magand, O., Borbon, A., Colomb, A., Bouvier, L., Baray, J.-L., Duflot, V., Ribeiro, M., Picard, D., Metzger, J.-M., Stamenoff, P., Benoit, Y., and Ah-Peng, C.: VELVET: an enclosure vegetation system to measure BVOC emission fingerprints in temperate and tropical climates, Frontiers in Environmental Science, 12, https://doi.org/10.3389/fenvs.2024.1372931, 2024.

Salignat, R., Américic, J., and Arteta, J.: UMR-CNRM/SURFEXv9.0-MEGANv3.2, https://doi.org/10.5281/ZENODO.21698653, 2026a.

Salignat, R., Américic, J., and Arteta, J.: SURFEXv9.0-MEGANv3.2 inputs, https://doi.org/10.5281/ZENODO.21699036, 2026b.

Salignat, R., Américic, J., and Arteta, J.: SURFEXv9.0-MEGANv3.2 outputs, https://doi.org/10.5281/ZENODO.21699207, 2026c.

Sarkar, C., Guenther, A. B., Park, J.-H., Seco, R., Alves, E., Batalha, S., Santana, R., Kim, S., Smith, J., Tóta, J., and Vega, O.: PTR-TOF-MS eddy covariance measurements of isoprene and monoterpene fluxes from an eastern Amazonian rainforest, Atmospheric Chemistry and Physics, 20, 7179–7191, https://doi.org/10.5194/acp-20-7179-2020, 2020.

Seco, R., Karl, T., Guenther, A., Hosman, K. P., Pallardy, S. G., Gu, L., Geron, C., Harley, P., and Kim, S.: Ecosystem-scale volatile organic compound fluxes during an extreme drought in a broadleaf temperate forest of the Missouri Ozarks (central <scp>USA</scp>), Global Change Biology, 21, 3657–3674, https://doi.org/10.1111/gcb.12980, 2015.

Sindelarova, K., Granier, C., Bouarar, I., Guenther, A., Tilmes, S., Stavrakou, T., Müller, J.-F., Kuhn, U., Stefani, P., and Knorr, W.: Global data set of biogenic VOC emissions calculated by the MEGAN model over the last 30 years, Atmospheric Chemistry and Physics, 14, 9317–9341, https://doi.org/10.5194/acp-14-9317-2014, 2014.

Sindelarova, K., Markova, J., Simpson, D., Huszar, P., Karlicky, J., Darras, S., and Granier, C.: High-resolution biogenic global emission inventory for the time period 2000–2019 for air quality modelling, Earth System Science Data, 14, 251–270, https://doi.org/10.5194/essd-14-251-2022, 2022.

https://doi.org/10.5194/egusphere-2026-5773
Preprint. Discussion started: 6 November 2026
© Author(s) 2026. CC BY 4.0 License.



Stavrakou, T., Müller, J.-F., Bauwens, M., De Smedt, I., Van Roozendael, M., Guenther, A., Wild, M., and Xia, X.: Isoprene emissions over Asia 1979–2012: impact of climate and land-use changes, Atmospheric Chemistry and Physics, 14, 4587–4605, https://doi.org/10.5194/acp-14-4587-2014, 2014.

Strada, S., Pozzer, A., Giuliani, G., Coppola, E., Solmon, F., Jiang, X., Guenther, A., Bourtsoukidis, E., Serça, D., Williams, J., and Giorgi, F.: Assessment of isoprene and near-surface ozone sensitivities to water stress over the Euro-Mediterranean region, Atmospheric Chemistry and Physics, 23, 13 301–13 327, https://doi.org/10.5194/acp-23-13301-2023, 2023.

Vermeuel, M. P., Novak, G. A., Kilgour, D. B., Claflin, M. S., Lerner, B. M., Trowbridge, A. M., Thom, J., Cleary, P. A., Desai, A. R., and Bertram, T. H.: Observations of biogenic volatile organic compounds over a mixed temperate forest during the summer to autumn transition, Atmospheric Chemistry and Physics, 23, 4123–4148, https://doi.org/10.5194/acp-23-4123-2023, 2023.

Wang, H., Lu, X., Seco, R., Stavrakou, T., Karl, T., Jiang, X., Gu, L., and Guenther, A. B.: Modeling Isoprene Emission Response to Drought and Heatwaves Within MEGAN Using Evapotranspiration Data and by Coupling With the Community Land Model, Journal of Advances in Modeling Earth Systems, 14, https://doi.org/10.1029/2022ms003174, 2022.

Wang, H., Liu, X., Wu, C., and Lin, G.: Regional to global distributions, trends, and drivers of biogenic volatile organic compound emission from 2001 to 2020, Atmospheric Chemistry and Physics, 24, 3309–3328, https://doi.org/10.5194/acp-24-3309-2024, 2024.

Wang, P., Chen, Y., Hu, J., Zhang, H., and Ying, Q.: Source apportionment of summertime ozone in China using a source-oriented chemical transport model, Atmospheric Environment, 211, 79–90, https://doi.org/10.1016/j.atmosenv.2019.05.006, 2019.